

# A Novel Range-spread Target Detection Algorithm Based on Waveform Entropy for Missile-borne Radar

Bo Liu, Wenge Chang, Xiangyang Li

School of Electronic Science and Engineering, National University of Defense Technology  
Changsha, 410073, P.R.China

liubo19830120@163.com, changwenge@nudt.edu.cn, lxyniu@sina.com

**Abstract**—A novel range-spread target detection algorithm in white Gaussian clutter for missile-borne radars is presented. For missile-borne radars, range migration of the target echoes during a coherent processing interval (CPI) is serious, which disperses the echo energy of the target and increases the difficulty of target detection. In this paper, range alignment for target echoes is accomplished in the frequency domain during the process of digital pulse compression. Then a range-spread detection algorithm based on the waveform entropy (WE) of the average combination of high range resolution profiles (HRRP) is addressed, which has the property of constant false-alarm rate (CFAR). Finally, the detection performance is assessed by Monte-Carlo simulation, and the results indicate that the detection performance of the proposed detector is superior to the traditional energy integrator and is robust for different HRRPs of the target.

**Keywords**—high range resolution; range-spread; waveform entropy; target detection; CFAR.

## I. INTRODUCTION

High range resolution (HRR) radars are widely used in precision guidance in recent years [1], for the echoes of HRR radars involve abundant target information and can be used for target recognition and accurate tracking [2]. For HRR radars, a relatively large target can be assumed to be the composition of multiple physical scatterers which distribute in different range cells in radar echo, so is called a range-spread target [3]. Consequently, traditional point-like target detection schemes for low range resolution (LRR) radars may fail for HRR radars [4]. Many achievements have been made in range-spread target detection during the past decades [5-9] (and references therein). Precisely, range-spread targets detection in white Gaussian noise of a known spectral density level is addressed in [5-6]. In [7], constant false-alarm rate (CFAR) detectors based on a generalized likelihood ratio test (GLRT) for range-spread targets are derived. Adaptive detection of distributed targets has been addressed in [8], with reference to Gaussian disturbance clutter. In [9], CFAR detection of distributed targets in non-Gaussian disturbance modelled as a compound-Gaussian process is studied. Nevertheless, the detection algorithms above do not consider the relative motion between the radar and the target, so they are not applicable in the scenario of moving range-spread target detection. In addition, some of them consume so much computation that they are difficult to implement in engineering.

In this paper, we propose a novel range-spread target detection algorithm for anti-ship terminal guidance HRR radars. Firstly, the range-spread target echo model of a missile-borne HRR chirp radar is established and the range alignment of HRRP is accomplished in the frequency domain.

Secondly, the range-spread target detection method based on the waveform entropy (WE) of the radar echo after coherent integration is addressed. Finally, the simulation indicates that the detection algorithm is superior to the traditional energy integrator detector and is robust for different HRRPs of the target. It should be pointed out that the proposed detector based on waveform entropy needs not to estimate the parameters of the clutter, which is a must for many traditional detection algorithms. Moreover, the computational complexity of the detector makes it suitable for missile-borne radar signal processing.

The paper is organized as follows. In Section II, we build and analyze the echo model of a range-spread target for missile-borne HRR radar. In Section III, range alignment of the target echoes is accomplished in the frequency domain. We address the range-spread target detection algorithm in Section IV. And the performance of the proposed method is assessed in Section V. At last, in Section VI, some conclusions are given.

## II. RADAR ECHO MODEL

The transmitted signal of a chirp radar is expressed as:

$$s(\hat{t}, t_s) = \text{rect}\left(\frac{\hat{t}}{T_p}\right) \cdot \exp(j\pi\mu\hat{t}^2) \cdot \exp(j2\pi f_c t) \quad (1)$$

where  $\hat{t}$  represents fast time;  $t_s = mT_r$  is slow time,  $m=0,1,\dots,M-1$ ,  $M$  is the number of pulses for coherent integration,  $T_r$  is the pulse repetition interval;  $t = \hat{t} + t_s$  is the absolute time;  $\mu = B/T_p$  is the frequency slope of chirp pulse,  $B$  is the signal's bandwidth,  $T_p$  is the pulse width;  $f_c$  is the carrier frequency.

According to the radar theory, the echo of a target is the convolution of the transmitted signal with the target range-scattering function. The range-scattering function of a static point-like target at the range of  $R_0$  can be written as [3]:

$$CF_0(t) = a_0 \cdot e^{j2\pi\varphi_0} \cdot \delta(t - 2R_0/c) \quad (2)$$

where  $a_0$  is the amplitude,  $\varphi_0$  is the initial phase, and  $c$  is the velocity of light. Thus the range-scattering function of a static range-spread target can be expressed as:

$$CF(t) = \sum_{k=1}^{K} a_k \cdot e^{j2\pi\varphi_k} \cdot \delta(t - \tau_k) \quad (3)$$

where  $K$  is the number of scattering centers of the range-spread target,  $a_k$ ,  $\varphi_k$  and  $\tau_k$  are the amplitude, initial phase and delay of the  $k$ -th physical scatterer of the range-spread target in range cell, respectively.

Assuming that the radar is working on tracking condition and moving towards the target at sea, and the radial velocity between the radar and the target remains constant during a coherent processing interval (CPI). Accordingly, the instantaneous range between the radar and the target is:

$$R_k(t_s) = R_{k0} - v \cdot t_s, k = 1, 2, \dots, K. \quad (4)$$

where  $R_k(\cdot)$  represents the instantaneous range of the  $k$ -th scatterer of the range-spread target,  $R_{k0}$  is the initial range of the  $k$ -th scatterer and  $v$  is the radial velocity between the radar and the target. Substituting (4) into (3), the instantaneous range-scattering function of a range-spread target is obtained:

$$\begin{aligned} CF(t, t_s) &= \sum_{k=1}^{k=K} a_k \cdot e^{j2\pi\phi_k} \cdot \delta \left[ t - \frac{2R_k(t_s)}{c} \right] \\ &= \sum_{k=1}^{k=K} a_k \cdot e^{j2\pi\phi_k} \cdot \delta \left[ t - \frac{2(R_{k0} - v \cdot t_s)}{c} \right]. \end{aligned} \quad (5)$$

Therefore, the radar echo of the range-spread target is expressed as:

$$\begin{aligned} r(\hat{t}, t_s) &= \sum_{k=1}^{k=K} a_k \cdot e^{j2\pi\phi_k} \cdot \text{rect} \left[ \frac{\hat{t} - 2(R_{k0} - v \cdot t_s)/c}{T_p} \right] \\ &\quad \cdot \exp \left\{ j\pi\mu \left[ \hat{t} - 2(R_{k0} - v \cdot t_s)/c \right]^2 \right\} \\ &\quad \cdot \exp \left\{ j2\pi(f_c + f_d) \left[ \hat{t} - 2(R_{k0} - v \cdot t_s)/c \right] \right\}. \end{aligned} \quad (6)$$

where  $f_d = 2vf_c/c$  is the Doppler frequency. After mixing and low-pass filtering, the baseband target echo is written as:

$$\begin{aligned} r_{\text{baseband}}(\hat{t}, t_s) &= \sum_{k=1}^{k=K} a_k \cdot e^{j2\pi\phi_k} \cdot \text{rect} \left[ \frac{\hat{t} - 2(R_{k0} - v \cdot t_s)/c}{T_p} \right] \\ &\quad \cdot \exp \left\{ j\pi\mu \left[ \hat{t} - 2(R_{k0} - v \cdot t_s)/c \right]^2 + \underbrace{j2\pi f_d \hat{t}}_{\text{time-frequency coupling}} \right\} \\ &\quad \cdot \exp \left\{ -j4\pi f_c (R_{k0} - v \cdot t_s)/c \right\}. \end{aligned} \quad (7)$$

From (7), it can be seen that the relative radial velocity between the radar and the target produces time-frequency coupling to the chirp signal [10], which results in mismatching between the target echo and the matched filter. After matched filtering, HRRPs of the range-spread target can be written as:

$$\begin{aligned} y(\hat{t}, t_s) &= \sum_{k=1}^{k=K} a_k \sqrt{\mu T_p^2} \cdot \text{rect} \left[ \frac{\hat{t} - 2(R_{k0} - v \cdot t_s)/c}{T_p} \right] \\ &\quad \cdot \frac{\sin \left\{ \pi B_c \left[ \hat{t} - \frac{2(R_{k0} - v \cdot t_s)}{c} - \frac{f_d}{\mu} \right] \cdot \left[ 1 - \frac{\hat{t} - 2(R_{k0} - v \cdot t_s)/c}{T_p} \right] \right\}}{\pi B_c \left[ \hat{t} - \frac{2(R_{k0} - v \cdot t_s)}{c} - \frac{f_d}{\mu} \right]} \\ &\quad \cdot \exp \left[ j2\pi \left( \phi_k + \frac{1}{8} \right) \right] \cdot \exp \left( -j4\pi f_c \cdot \frac{R_{k0} - v \cdot t_s}{c} \right) \\ &\quad \cdot \exp \left\{ -j\pi\mu \left[ \hat{t} - \frac{2(R_{k0} - v \cdot t_s)}{c} \right] \right\}. \end{aligned} \quad (8)$$

Due to mismatching, envelopes of the pulse compression results in (8) are not sinc functions any more. According to [10], the amplitude loss in (8) is negligible, while the time shift resulting from the time-frequency coupling of chirp signal is significant and will affect range measurement accuracy. From (8), the time shift of the target resulting from the time-frequency coupling of the chirp signal is:

$$\Delta t = f_d / \mu. \quad (9)$$

Additionally, the radial velocity  $v$  between the radar and the target produces range migration during a CPI. From (8), the migration time between the adjacent pulses is expressed as:

$$t_m = 2vT_r / c. \quad (10)$$

The range migration factor  $P$  is defined as:

$$P = B(M-1)t_m = 2Bv(M-1)T_r / c. \quad (11)$$

The range migration factor  $P$  represents the number of the range resolution cells that the target echo spreads during the CPI.

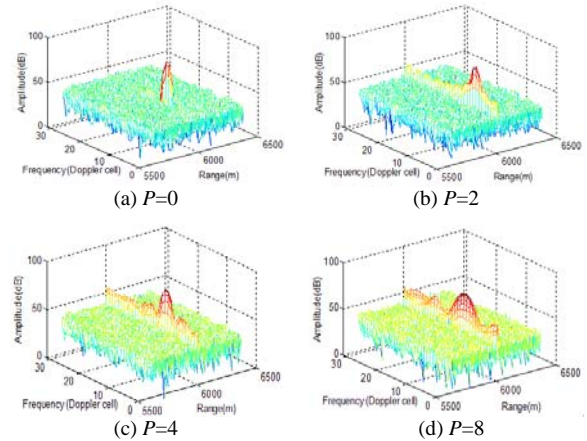


Figure 1. Range migration effects on coherent integration results. Simulation parameters:  $B = 80\text{MHz}$ ,  $M = 32$ ,  $T_p = 20\mu\text{s}$ ,  $T_r = 250\mu\text{s}$ , sampling rate  $f_s = 120\text{MHz}$ .

Coherent integration is widely adopted to enhance the signal-to-noise ratio (SNR) of radar echo [11], which improves the target detection performance of the radar system. But when there is high speed relative motion between the radar and the target, the range migration will affect the result of coherent integration. Fig. 1 shows the range migration effects on coherent integration results of a point-like target with range migration factor  $P=0, 2, 4$  and  $8$ , respectively. It can be seen that the range migration disperses the echo energy of the target in coherent integration and so makes it more difficult to target detection.

Assuming it is required that the range migration during the CPI should be no more than half of the range resolution cell [12], according to (11), the radial velocity between the radar and the target should satisfy the following equation:

$$|v| < \frac{c}{4B(M-1)T_r}. \quad (12)$$

### III. RANGE ALIGNMENT

For missile-borne radar, equation (12) usually can not be satisfied. Therefore it is necessary to correct the range migration between the HRRPs before coherent integration. Supposing the velocity of the missile  $v_m$  can be obtained by the missile-borne inertial navigation system (INS) [13], the velocity measurement error is  $\Delta v_m$ . If we adopt  $v_m$  as an estimation of the radial velocity between the radar and the target, the estimation error is:

$$\varepsilon = \Delta v_m + v_r. \quad (13)$$

where  $v_t$  is the radial velocity of the target ship. For the time being, the radial velocity estimation error  $\varepsilon$  generally satisfies (12) and so  $v_m$  can be employed to correct the range migration between the HRRPs during a CPI.

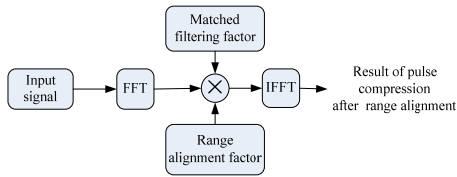
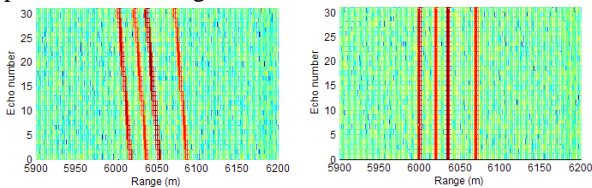


Figure 2. Range alignment during the digital pulse compression

By utilizing the time-frequency symmetry properties of the Fourier transform, range alignment can be accomplished in the frequency domain. Firstly, transform the pulse compression results in (8) to the frequency domain by the Fourier transform (FT) in the fast time dimension. Then multiply them by the corresponding the frequency domain phase terms related to the radial velocity estimation  $v_m$ . Finally, transform the products to the time domain by the inverse Fourier transform (IFT) and the result of range alignment is obtained:

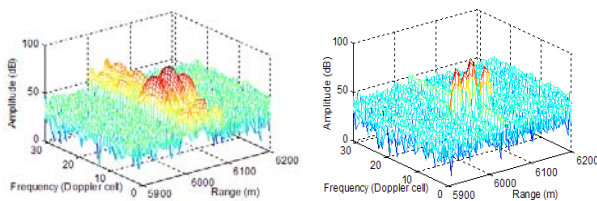
$$\begin{aligned}
 y'(\hat{t}, t_s) &= IFT \left\{ y(f, t_s) \cdot \exp \left[ j4\pi v_m \frac{(f_c / \mu - t_s) \cdot f}{c} \right] \right\} \\
 &\approx \sum_{k=1}^{k=K} a_k \sqrt{\mu T_p^2} \cdot \text{rect} \left[ \frac{\hat{t} + f_d / \mu - 2R_{k0} / c}{T_p} \right] \cdot \text{sinc} \left[ \pi B \left( \hat{t} - \frac{2R_{k0}}{c} \right) \right] \\
 &\quad \cdot \exp \left[ j2\pi \left( \varphi_k + \frac{1}{8} \right) \right] \cdot \exp \left( -j4\pi f_c \cdot \frac{R_{k0} - v \cdot t_s}{c} \right) \\
 &\quad \cdot \exp \left[ -j\pi \mu \left( \hat{t} - 2R_{k0} / c + f_d / \mu \right) \right]. \quad (14)
 \end{aligned}$$

where  $y'(\hat{t}, t_s)$  is the HRRPs after range alignment,  $y(f, t_s) = FT[y(\hat{t}, t_s)]$ ,  $f$  is the natural frequency. Although the process of the range alignment above needs abundant computation, it does not take much additional time in the signal processing, because it could be accomplished concurrently with digital pulse compression. Fig. 2 is the flow chart of the range alignment scheme during the pulse compression with a digital matched filter.



(a) Without range alignment,  $P=8.27$  (b) After range alignment,  $P=0.041$

Figure 3. Top view of target echoes after pulse compression. Radar parameters:  $B = 80\text{MHz}$ ,  $M = 32$ ,  $T_p = 20\mu\text{s}$ ,  $T_r = 250\mu\text{s}$ .



(a) Without range alignment (b) After range alignment.

Figure 4. Coherent integration results of the echoes shown in Fig. 3.

Supposing the velocity of the missile  $v_m$  provided by the INS is 2000 m/s, the real radial velocity between the missile and the target  $v = 2020$  m/s, the error of the coarse estimation of the radial velocity  $\varepsilon = 20$  m/s. The echoes of a range-spread target with four scattering centers are shown in Fig. 3, the horizontal is the range axis, and the ordinate is the Doppler frequency axis, where Fig. 3 (a) shows the echoes without range alignment, Fig. 3 (b) shows the echoes after range alignment. Fig. 4 shows the coherent integration results of the target echoes before and after range alignment. It can be seen, compared with the coherent integration result without range alignment, the echo energy of the target has been effectively gathered after range alignment.

#### IV. TARGET DETECTION

After Range alignment and coherent integration, the echo energy of the range-spread target is accumulated effectively. Denoting the data after coherent integration by matrix  $Z \{M \times N\}$ , where  $N$  is the maximum of the range cells number that the desired target spreads. The detection problem can be formulated in terms of the following binary hypotheses test:

$$\begin{cases} H_0 : z_m = w_m \\ H_1 : z_m = x_m + w_m \end{cases}, m = 0, 1, \dots, M-1. \quad (15)$$

where  $z_m$ ,  $w_m$ ,  $x_m$  are the received signal vector, sea clutter vector, and HRRP of the desired target, respectively. All of them are row vectors with length  $N$ , and  $w_m$  is assumed to be zero-mean complex white Gaussian noise.

In practical applications, to restraint the side lobe of the Doppler [14], a weighting function is generally adopted during coherent integration, which expands the Doppler of the target echo. Moreover, the target ship may corner sometimes, which expands the Doppler as well. Nevertheless, the maximum number of Doppler cells that the target echo spreads in Doppler axis usually can be known in advance. Setting a sliding-window of width  $M_0 \cdot r_d$  on the Doppler axis, where  $M_0$  is the max number of the Doppler cell that the target echo may take up,  $M_0 \leq M$ , and  $r_d$  is the Doppler resolution cell of the radar system. The echo energy within the window is integrated, whichever makes the integrated value of the largest window is chosen as the target detection window, denoted by  $W$ . The detection problem can be redescribed as the following binary hypothesis test:

$$\begin{cases} H_0 : z_m(n) = w_m(n) \\ H_1 : z_m(n) = x_m(n) + w_m(n) \end{cases} \quad (16)$$

$$m = m_0, m_0 + 1, \dots, m_0 + M_0 - 1, n = 0, 1, \dots, N - 1.$$

where  $m_0$  is the starting Doppler cell number in  $W$ . Envelops of the  $M_0$  HRRPs are high correlated, which can be utilised to construct the detector. An average combination of the radar echo within the detection window  $W$  is defined by:

$$A(n) = \frac{1}{M_0} \sum_{m=m_0}^{m_0+M_0-1} z_m^2(n), n = 0, 1, \dots, N - 1. \quad (17)$$

In fact, the average combination defined in the above equation can be seen as incoherent integration of the  $M_0$  echoes. Because of the independence of the clutter for

different echoes,  $A(n)$  has higher signal-to-clutter (SCR) than single echo. In other words,  $A(n)$  is much sparser than the single echo owing to incoherent integration. Here, the entropy concept is introduced to measure the sparseness of the waveform of  $A(n)$ , which is named as the waveform entropy (WE) [15]. Entropy is a measure of the uncertainty of random variables [16], in order to adopt the concept of entropy, setting:

$$\begin{cases} p(n) = |A(n)| / \|A\| \\ \|A\| = \sum_{n=0}^{N-1} |A(n)| \end{cases}, n = 0, 1, \dots, N-1. \quad (18)$$

the WE of  $A(n)$  is defined as:

$$WE[A(n)] = - \sum_{n=0}^{N-1} p(n) \cdot \log_2 p(n). \quad (19)$$

According to the definition above, the waveform entropy has the following properties:

- (1)  $E[A(n)] \rightarrow 0$ , when  $p(n) \rightarrow 0$ . The sparser  $A(n)$  is, the smaller  $WE[A(n)]$  is.
- (2)  $E[A(n)] \leq \log_2 N$ , the equation comes into existence when  $p(n) = 1/N, \forall n = 0, 1, \dots, N-1$ . The more homogeneous the distribution of  $A(n)$ 's energy is, the larger  $WE[A(n)]$  will be.

Accordingly, if the energy of a waveform distributes uniformly along its parametric axis, the WE reaches the maximum. On the contrary, if the energy concentrates only on single sampling point of the waveform, the WE is the minimum.

For the average combination of the radar echo  $A(n)$ , when the target is absent, the energy of the Gaussian clutter echo distributes uniformly, which results in a larger value of  $WE[A(n)]$ . Whereas, when the target is present, the energy of the target echo appears in a number of isolated range cells, the sparseness of  $A(n)$  corresponds to a low value of  $WE[A(n)]$ .

Therefore, the WE of  $A(n)$  can distinguish the clutter sequences and target plus clutter sequences effectively. Fig. 5 shows the waveform entropies of  $A(n)$  while the target is absent and present, respectively. The horizontal is the trail number, and the ordinate is the waveform entropy.

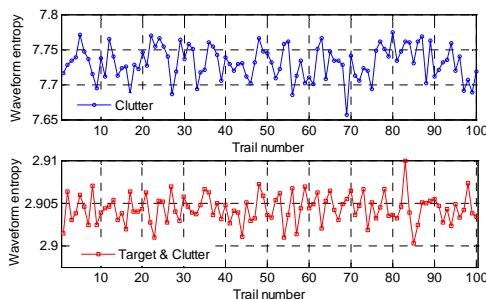


Figure 5. Waveform entropies of  $A(n)$  when the target is absent (above) and present (below). Simulation parameters:  $M = 32, M_0 = 4, N = 256, SCR = 30dB$ .

Thus, the detection statistic of the detector is defined as:

$$R = WE[A(n)] = WE \left[ \frac{1}{M_0} \sum_{m=m_0}^{m_0+M_0-1} z_m^2(n) \right]_{H_0}^{H_1} \lesseqgtr T. \quad (20)$$

where  $T$  is the detection threshold,  $n = 0, 1, \dots, N-1$ .

Under the  $H_0$  hypothesis in (16), the detection statistic is written as:

$$R = WE \left[ \frac{1}{M_0} \sum_{m=m_0}^{m_0+M_0-1} w_m^2(n) \right], n = 0, 1, \dots, N-1. \quad (21)$$

Setting:

$$q(n) = \frac{\sum_{m=m_0}^{m_0+M_0-1} w_m^2(n)}{\sum_{n=0}^{N-1} \sum_{m=m_0}^{m_0+M_0-1} w_m^2(n)}, n = 0, 1, \dots, N-1. \quad (22)$$

Then, the detection statistic under the  $H_0$  hypothesis is expressed as:

$$R = - \sum_{n=0}^{N-1} q(n) \cdot \log_2 q(n). \quad (23)$$

Here, we assume the variance of  $w_m(n)$  is  $\sigma^2$ . Then,  $\frac{1}{\sigma^2} w_m^2(n)$  is in chi-square distribution with freedom 2, namely,

$$\frac{1}{\sigma^2} w_m^2(n) \sim \chi^2(2). \quad (24)$$

where  $\chi^2(l)$  denotes a chi-square distribution with freedom  $l$ . Similarly,

$$\frac{1}{\sigma^2} \sum_{m=m_0}^{m_0+M_0-1} w_m^2(n) \sim \chi^2(2M_0), n = 0, 1, \dots, N-1. \quad (25)$$

and,

$$\frac{1}{\sigma^2} \sum_{n=0}^{N-1} \sum_{m=m_0}^{m_0+M_0-1} w_m^2(n) \sim \chi^2(2M_0N). \quad (26)$$

From (22), (25) and (26), we can obtain:

$$N \cdot q(n) \sim F(2M_0, 2M_0N), n = 0, 1, \dots, N-1. \quad (27)$$

So the probability distribution function (PDF) of  $q(n)$  is independent of the clutter variance  $\sigma^2$ . Therefore, from (23), we can find that the detection statistic  $R$  under the  $H_0$  hypothesis is also independent of  $\sigma^2$ . Thus, the false alarm probability is independent of the external clutter environment, which implies that the proposed detector in (20) is a CFAR detector.

The Neyman-Pearson criterion is employed to make the judgement. Although the closed-form expression for the false-alarm probability ( $p_{fa}$ ) is difficult to derive, the threshold for a special false-alarm probability can be obtained by the widely used Monte-Carlo method. While the detection statistic is smaller than the threshold,  $H_1$  hypothesis is selected.

## V. PERFORMANCE ASSESSMENT

In this section, we assess the performance of the waveform entropy detector given by (20) resorting to Monte-Carlo simulations. The simulation parameters of the radar are listed in table 1, which are assumed according to the principle in [1].

Fig. 6 shows the HRRPs of two range-spread targets simulated by the computer, where HRRPs of target 1 and target 2 are shown in Fig. 6(a) and Fig. 6(b), respectively. Each of the two targets has four scattering centers, while the distributions of the scattering centers are different.

TABLE I. PARAMETERS OF A HRR CHIRP RADAR

$B$	$T_r$	$T_p$	$M$	$f_s$
80 MHz	250 $\mu$ s	20 $\mu$ s	32	120MHz

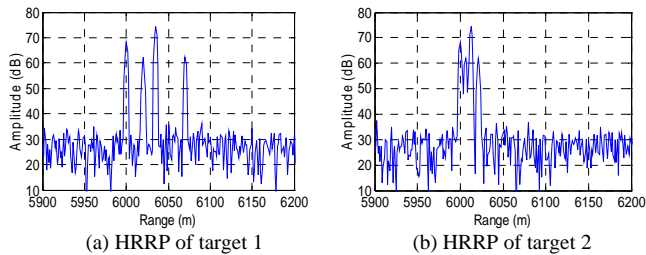


Figure 6. HRRPs of two targets simulated by computer

In the following we compare the performance of the proposed detector based on waveform entropy with the integrator detector [5]. Gaussian clutter is generated by computer, while the variance is adjusted to SCR. Taking the computational complexity into account, we assumed  $p_{fa} = 0.0001$ , and 1000 independent trials are carried out at each SCR.

Fig. 7 shows the detection performance of the proposed detector based on waveform entropy and the integrator detector. Simulations for target 1 and target 2 are shown in Fig. 7(a) and Fig. 7(b), respectively. It can be seen that the detection performance of the proposed detector is superior to the integrator detector.

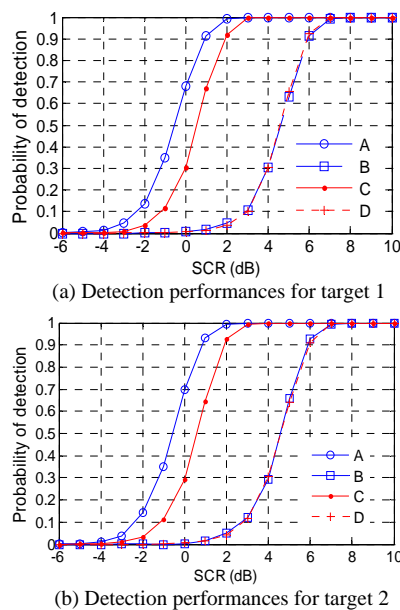


Figure 7. Detection performance of two detectors for target 1 and target 2. ( $p_{fa} = 0.0001, M = 32, N = 256$ . A: The proposed detector,  $M_0 = 4$ ; B: The integrator detector,  $M_0 = 4$ ; C: The proposed detector,  $M_0 = 8$ ; D: The integrator detector,  $M_0 = 8$ .)

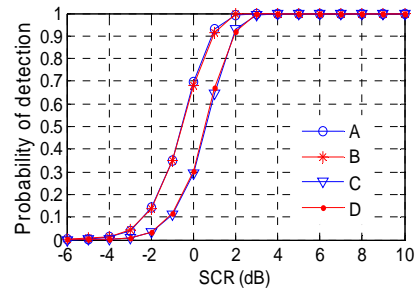


Figure 8. Detection performance of the proposed detector based on waveform entropy for the two targets. ( $p_{fa} = 0.0001, M = 32, N = 256$ . A: Target 1,  $M_0 = 4$ ; B: Target 2,  $M_0 = 4$ ; C: Target 1,  $M_0 = 8$ ; D: Target 2,  $M_0 = 8$ .)

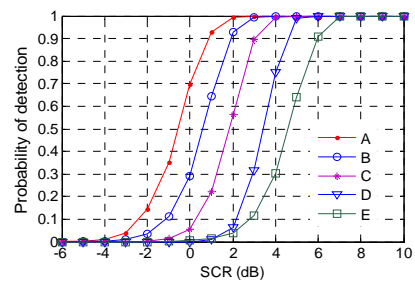


Figure 9. Detection performance for target 2 with different  $M_0$ . ( $p_{fa} = 0.0001, M = 32, N = 256$ . A: The proposed detector,  $M_0 = 4$ ; B: The proposed detector,  $M_0 = 8$ ; C: The proposed detector,  $M_0 = 16$ ; D: The proposed detector,  $M_0 = 32$ ; E: The integrator detector.)

The detection performance of the proposed detector for target 1 and target 2 with different Doppler distributions ( $M_0$ ) is shown in Fig. 8. From Fig. 8, we can see that the detection performance of the proposed detection method is robust to the HRRP of the desired target, and yet is connected with the Doppler distribution of the target. Fig. 9 illustrates the relationship between the detection performance of the proposed detector and the Doppler distribution of the target echo. As can be seen, the detection performance of the proposed detector decreases while the Doppler of the target spreads. In this simulation, the detection performance of the proposed detector decreases 1 dB while  $M_0$  doubles. In spite of this, the detection performance of the proposed detector is superior to the integrator detector even when  $M_0 = M$ .

## VI. CONCLUSION AND FUTURE WORK

HRR radars are widely used in precision guidance in recent years, for the echoes of HRR radars involve abundant target information and can be used for target recognition and accurate tracking. This paper presents a novel range-spread target detection algorithm for missile-borne HRR radars. Firstly, the range-spread target echo model of missile-borne HRR chirp radar is established and the range alignment of HRRP is accomplished in the frequency domain. Then a CFAR range-spread detection algorithm based on the WE of the average combination of the HRRPs is addressed. The simulation indicates that the detection algorithm is superior to the traditional energy integrator and is robust for different

HRRPs of the target. The proposed detector based on WE needs not to estimate the parameters of the clutter, and the computational complexity of the detector makes it suitable for missile-borne radar signal processing. Future work will focus on the practical application of the proposed algorithm, and the target detection performance will be further tested by using the measured data.

## REFERENCES

- [1] Wehner, D.R., *High-Resolution Radar*, Boston: Artech House, 1995, Ch.p4-Ch.p5.
- [2] B. Liu and W. Chang, "A novel range-spread target detection approach for frequency stepped chirp radar," *Progress In Electromagnetics Research*, vol. 131, 2012, pp. 275-292. doi:10.2528/PIER.12062510.
- [3] L. Du, H. W. Liu, and Z. Bao, "Radar HRRP target recognition based on higher-order spectra," *IEEE Trans. Signal Process.*, vol. 53(7), 2005, pp. 2359-2368.
- [4] Gerard A. Van. Der. Spek, "Detection of a distributed target," *IEEE Transactions on Aerospace and Electronics Systems*, vol. AES-7(5), 1971, pp. 922-931.
- [5] P. K. Hughes II., "A high-resolution radar detection strategy," *IEEE Transactions on Aerospace and Electronics Systems*, vol. AES-19(5), 1983, pp. 663-667.
- [6] Karl Gerlach, Michael Steiner, and F. C. Lin, "Detection of a spatially distributed target in white noise," *IEEE Signal Processing Letters*, vol. 4(7), 1997, pp. 198-200.
- [7] E. Conte, A. De. Maio, and G. Ricci, "GLRT-based detection algorithms for range-spread targets," *IEEE Transactions on Signal Processing*, vol.49(7), 2001, pp. 1336-1348.
- [8] Karl Gerlach and M. J. Steiner, "Adaptive detection of range distributed targets," *IEEE Transactions on Signal Processing*, vol. 47(7), 1999, pp. 1844-1851.
- [9] E. Conte and A. De. Maio, "Distributed targets detection in compound-Gaussian noise with Rao and Wald tests," *IEEE Transactions on Aerospace and Electronic Systems*, vol. 51, Apr, 2003, pp. 568-582.
- [10] Xiaofeng Song, "Effect of Doppler Frequency Shift on Linear Frequency Modulation Signal Pulse Compression," *Electronic Science and Technology*, vol. 22 (4), 2009, pp. 42-44.
- [11] David K. Barton and Sergey A. Leonov, *Radar Technology Encyclopedia (Electronic Edition)*, Boston: Artech House, 1998, pp. 217-222.
- [12] Huixia Sun, Zheng Liu, and Yunhe Cao, "Estimation of a high-velocity target's motion parameters for a modulated frequency stepped radar," *Journal of Xidian University*, vol. 38(1), 2011, pp. 136-141.
- [13] T.A. Moore et. al., "Use of the GPS Aided Inertial Navigation System in the Navy Standard Missile for the BMDO/Navy LEAP Technology Demonstration Program", *Proceedings of ION GPS-95*, Palm Springs, CA, September 12-15, 1995.
- [14] George W. Stimson, "Introduction to Airborne Radar" (Second Edition), Raleigh: SciTech Publishing, Inc, 1998, Ch.p18-Ch.p19.
- [15] S. Xu, P. Shui, and X. Yan, "CFAR detection of range-spread target in white Gaussian noise using waveform entropy," *Electronics Letters*, vol. 46(9), 2010, pp. 647-649.
- [16] L.M. Martyushev and V.D. Seleznev, "Maximum entropy production principle in physics, chemistry and biology," *Physics Reports*, 426, 2006, pp. 1-45.

## ACKNOWLEDGMENT

The authors wish to thank the editors, reviewer 1, reviewer 2, reviewer 3, reviewer 4, and reviewer 5, whose comments and suggestions helped to improve the contents of the paper.